Magnetic and crystal structure of $Ho_5(Si_xGe_{1-x})_4$ studied by neutron diffraction

C. Ritter,[1] C. Magen,[2,*] L. Morellon,[3,4] P. A. Algarabel,[4] M. R. Ibarra,[3,4] A. M. Pereira,[5] J. P. Araujo,[5] and J. B. Sousa[5]

[1]*Institut Laue-Langevin, Boîte Postale 156, 38042 Grenoble Cédex 9, France*

[2]*Instituto de Nanociencia de Aragón-ARAID, Universidad de Zaragoza, 50009 Zaragoza, Spain*

[3]*Instituto de Nanociencia de Aragón, Universidad de Zaragoza, 50009 Zaragoza, Spain*

[4]*Instituto de Ciencia de Materiales de Aragón, Universidad de Zaragoza and Consejo Superior de Investigaciones Científicas, 50009 Zaragoza, Spain*

[5]*IFIMUP and IN–Institute of Nanoscience and Nanotechnology, Departamento de Física, Faculdade de Ciências, Universidade do Porto, Rua do Campo Alegre, 4169-007 Porto, Portugal*

(Received 31 March 2009; revised manuscript received 31 July 2009; published 23 September 2009)

The magnetic and crystal structures of the magnetocaloric $Ho_5(Si_xGe_{1-x})_4$ ($x=1$, 0.75, 0.5 and 0) have been studied by neutron powder diffraction experiments. The room-temperature crystal phases of the compositions $x=1$, 0.75, and 0.5 are preserved in the whole temperature range 2–300 K, i.e. the Gd_5Si_4-type *Pnma* O(I) structure for Ho_5Si_4, the $Gd_5Si_2Ge_2$-type $P112_1/a$ M state in $x=0.75$, and the Sm_5Ge_4-type *Pnma* O(II) phase in $x=0.5$. Ho_5Si_4 undergoes a second order ferromagnetic (FM) transition at $T_C=77$ K into a noncollinear FM structure with the magnetization oriented mainly along the *a* axis and weak antiferromagnetic (AFM) coupling along *b* and *c* (magnetic space group $Pnm'a'$). Ho_5Si_3Ge becomes FM at $T_C=50$ K (magnetic space group $P112_1'/a$). At $T_C'\sim 16$ K an incipient second incommensurate magnetic phase appears which becomes commensurate below 8 K with a propagation vector $\mathbf{k}=(0\ 0\ \frac{1}{4})$. The magnetic structure of the main phase at 30 and 2 K shows the dominance of a FM coupling along the *a* axis with an AFM canting along *c*. $Ho_5Si_2Ge_2$ stands out for the complexity of its low-temperature magnetic structure. In addition to the Néel transition of the O(II) phase at $T_N\sim 30$ K (magnetic space group $Pn'm'a'$), two additional magnetic phases with propagation vectors $\mathbf{k}=(0\ 0\ \frac{1}{4})$ and $\mathbf{k}=(\frac{1}{2}\ 0\ 0)$ appear at 15 and 12 K, respectively. In Ho_5Ge_4 the main O(II) structure orders AFM with $\mathbf{k}=(0\ 0\ 0)$ at $T_N\sim 30$ K in the same magnetic space group $Pn'm'a'$. Below 25 K a complete structural transition from high temperature O(II) *Pnma* to $P2_1/m$ takes place within the AFM state. The magnetic structure of this new nuclear phase stays AFM with $\mathbf{k}=(0\ 0\ 0)$, but sees two out of six independent Ho sites non magnetic. A second magnetic transition takes place at about 18 K characterized by the appearance of a second propagation vector $\mathbf{k}=(0\ 0\ \frac{1}{2})$ which magnetically couples the formerly non magnetic Ho sites. Magnetic-field dependent neutron diffractograms demonstrate that FM sets in in Ho_5Ge_4. The onset of ferromagnetism is associated with the previously reported nucleation of a new high field O(II) *Pnma* phase. Contrary to the intensity of the magnetic coupling with the propagation vector $\mathbf{k}=(0\ 0\ 0)$, which disappears quickly with the onset of FM, a progressive decrease of the intensity associated with the state $\mathbf{k}=(0\ 0\ \frac{1}{2})$ suggests a possible relationship between the extent of the magnetic coupling $\mathbf{k}=(0\ 0\ \frac{1}{2})$ and the percentage of remnant $P2_1/m$ phase.

DOI: 10.1103/PhysRevB.80.104427 PACS number(s): 75.25.+z, 75.30.Kz, 75.50.Cc

I. INTRODUCTION

The $R_5(Si_xGe_{1-x})_4$ compounds (R=rare earth) have become during the last decade one of the most amazing systems among the intermetallic materials. The most extraordinary discovery made on these materials is the giant magnetocaloric effect (GMCE),[1–3] but the $R_5(Si_xGe_{1-x})_4$ compounds also exhibit giant magnetoresistance[4,5] and magnetostriction,[5,6] anomalous Hall effect and atypical transport properties,[7–9] irreversibility and relaxation effects in structural transformations,[10,11] the onset of exotic magnetic phases,[12,13] and an unusually strong effect of hydrostatic pressure on its physical properties.[14,15] This unprecedented amount and variety of uncommon properties is intimately related with the peculiar crystal structure and its interplay with the magnetic and electronic properties. The system is characterized by a layered structure composed of virtually rigid slabs that, when magnetically ordered, present a ferromagneticlike state. The overall magnetic, crystallographic, and electronic properties are eventually determined by the distance and chemical bonding between the neighboring slabs, which can be modified by changing the rare earth ions and the Si/Ge doping, or the extrinsic parameters as temperature, magnetic field and hydrostatic pressure.[1–6,14,15] Other factors such as the level of impurities and the sample preparation conditions are also key factors in the macroscopic and microscopic properties of this system.[16,17]

Due to the richness of factors relevant for the properties of these compounds, a comprehensive and detailed physical characterization is needed. Although some series have been widely investigated, especially with R=Gd, Tb, and Er, there is a lack of experimental evidence in many other members of the family such as $Ho_5(Si_xGe_{1-x})_4$. Scarce macroscopic characterization has been performed since Holtzberg *et al.* reported the basic magnetic and structural properties of the parent compounds Ho_5Si_4 and Ho_5Ge_4 in 1967.[18,19] Recently, the temperature-composition phase diagram of the series has been determined from room-temperature x-ray diffraction, temperature dependent magnetization and linear thermal expansion (LTE).[20] As a result, we know that the composition

range $0 \leq x \leq 0.5$ crystallizes in the Sm_5Ge_4-type O(II) state at room temperature and the system orders antiferromagnetically (AFM) at a Néel temperature (T_N) between 25 and 30 K as a function of x. For $0.75 \leq x \leq 0.875$, a purely monoclinic $Gd_5Si_2Ge_2$-like M structure is found, which undergoes a ferromagnetic (FM) transition at Curie temperatures (T_C) increasing with composition from $T_C=49$ to 57 K. Finally, the holmium silicide is the only compound studied which presents the Gd_5Si_4 structure—labeled O(I)—at room temperature and orders FM at $T_C=77$ K. All the compounds present below their ordering temperatures additional magnetic anomalies.

None of the compositions studied have shown evidence of structural changes below room temperature except Ho_5Ge_4, in which a small LTE anomaly have been detected at very low temperature (~17 K), which might be the fingerprint of an incipient structural transition. A very recent work published by Singh *et al.* has demonstrated the existence of a structural transformation concomitant with the Néel transition at $T=23$ K, supported both experimentally and theoretically by first principles calculations.[21] Surprisingly a novel monoclinic phase of space group $P2_1/m$ ($P12_1/m1$ in Singh's work), previously unknown to exist in the $R_5(Si_xGe_{1-x})_4$ family of compounds, appears at this transition. This new monoclinic phase is characterized by a monoclinic distortion in the *ac* plane instead of the usual *ab* plane commonly known in these compounds. The accompanying small positive volume change of ~0.1% with no change in the interlayer bonding distances contradicts the previous knowledge on the temperature dependence of the crystal phase and interlayer bonding behavior in these materials. Low-temperature magnetostriction isotherms have demonstrated that a sharp anomaly can be induced by the application of an external magnetic field.[20] The nature of this anomaly has been clarified in the Singh's work, where x-ray diffraction experiments as a function of the magnetic field have revealed the onset of a partial magnetic-field induced structural transformation into a O(II) state with an addition volume cell increase of ~0.7% (~30% at 3.5 T). Regarding the microscopic characterization of the magnetic structure, to the best of our knowledge the only study devoted to the determination of the low-temperature magnetic and crystal structure has been carried out by Schobinger-Papamantellos and Niggli in Ho_5Ge_4,[22] who reported the onset of a three dimensional canted commensurate structure at $T_N \sim 21$ K with the magnetic space group $Pn'm'a'$. Below 18 K a second magnetic phase sets in with a propagation vector $\mathbf{k}=(\frac{1}{2}\ 0\ 0)$ which was thought to belong to a second nuclear phase coexisting with the main one at low temperature. In the light of recent discoveries on the low-temperature crystal structures and transformations in Ho_5Ge_4, the role of this novel monoclinic state in the magnetic state at low temperature and the microscopic description of the field-induced structural and magnetic transformation have not been clarified yet. Furthermore, the possible existence of the monoclinic $P2_1/m$ crystal state in other compositions of the Ho series is to be determined. In order to shed new light in all this questions, this work provides a detailed description of the magnetic and crystal structure of the whole $Ho_5(Si_xGe_{1-x})_4$ system at low temperature by means of neutron powder diffraction experiments in selected compositions representative of the three solid solution regions described above.

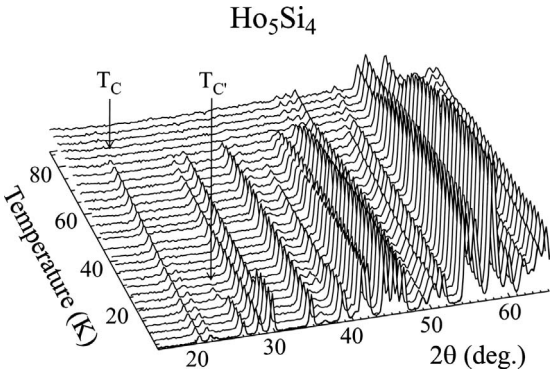

FIG. 1. Neutron D1B thermodiffractogram of Ho_5Si_4 in the low-angle regime where the magnetic reflections are strong.

II. EXPERIMENT

Polycrystalline specimens of Ho_5Si_4, Ho_5Si_3Ge, $Ho_5Si_2Ge_2$, and Ho_5Ge_4 have been synthesized by the arc-melting of stoichiometric mixtures of high-purity Ho (99.99 wt. %), and high-purity Si and Ge (99.9999 wt. %) purchased from commercial vendors. Further details on the sample preparation and characterization can be found elsewhere.[20]

Neutron diffraction experiments have been carried out in the high intensity powder diffractometer D1B ($\lambda=2.52$ Å) and the high resolution powder diffractometers D1A ($\lambda=1.908$ Å) and D2B ($\lambda=1.59$ Å) at the Institute Laue-Langevin (ILL) in Grenoble (France). Temperature scans have been measured on D1B in the temperature range 2–300 K. Neutron diffraction patterns have been collected at selected temperatures and angles between $2\theta=5°$ and 158° on D1A. D2B was used to measure the magnetic-field dependence of the diffraction pattern of Ho_5Ge_4. Crystallographic and magnetic structures have been refined by analyzing the neutron diffraction patterns collected in D1A with the Rietveld-method software package FULLPROF.[23]

III. RESULTS AND DISCUSSION

A. Ho_5Si_4

The neutron thermodiffractogram of Ho_5Si_4 collected in D1B in the temperature range 2–300 K shows no significant change of the nuclear diffraction pattern when cooling down to the magnetic ordering temperature of $T_C=77$ K, so the system remains in the *Pnma* O(I) phase in the paramagnetic (PM) state. A close-up of the low-temperature low-angle D1B thermodiffractogram is plotted in Fig. 1. The appearance of new peaks is evidenced at $T \sim 75$ K at low angles and the simultaneous increase of the intensity of some nuclear Bragg peaks is indicative of the onset of FM ordering with a significant AFM component. Below $T_C' \sim 22$ K small additional magnetic peaks appear which change their 2Θ position at about 16 K. These magnetic peaks are asso-

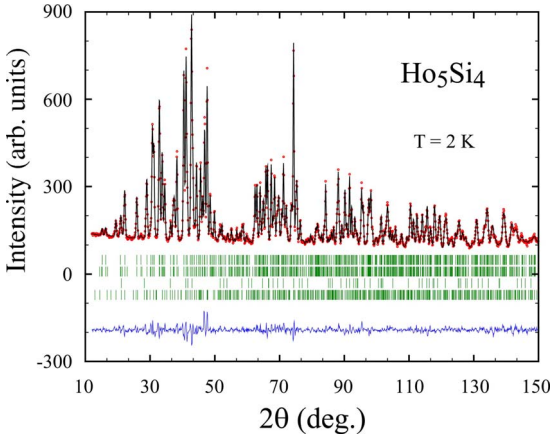

FIG. 2. (Color online) High resolution neutron powder diffraction pattern of Ho_5Si_4 at $T=2$ K collected on the D1A diffractometer. The experiment (dots), the refinement (line) and their difference (line at the bottom) are represented. The vertical bars mark the reflections related to, from top to bottom, the main (structural) phase, the magnetic part of the main phase, the impurity (structural) phase, and the magnetic part of the impurity.

ciated to a small amount of impurity phase HoSi (space group *Cmcm*) which adopts first an incommensurate structure before becoming commensurate at about 16 K. The main Ho_5Si_4 phase does not show any additional changes down to the base temperature of 2 K. The magnetic structure of the impurity phase has been described by Nguyen *et al.*,[24] our refinement of the 2 K data of Ho_5Si_4 included the nuclear and magnetic contributions of this impurity phase (about 7 wt. %). Therefore, we have to conclude that the spin reorientation transition reported at $T_{SR}=17$ K by Pereira *et al.* from magnetization experiments on the same sample is in reality connected to the magnetism of the impurity phase.[20]

A detailed Rietveld analysis has been performed on diffraction patterns collected at selected representative temperatures in the high resolution diffractometer D1A in order to refine the crystal structure and magnetic ordering at low temperature. Figure 2 shows the refinement of the pattern collected at the lowest temperature ($T=2$ K). A summary of the crystallographic parameters and the magnetic moment components obtained from the refinements at 100, 30 and 2 K are listed in Tables I and II, respectively. The nuclear Bragg scattering has been successfully fitted to the *Pnma* Gd_5Si_4-type O(I) phase found at room temperature in all cases without need of any other 5:4 nuclear component, confirming that Ho_5Si_4 crystallizes in the O(I) state in the whole range of temperatures. The magnetic space groups associated with the crystallographic space group *Pnma* for a propagation vector $\mathbf{k}=(0\ 0\ 0)$ can be determined by magnetic symmetry analysis. Programs such as BASIREPS or SARAH do this nowadays automatically.[23,25] The allowed magnetic space groups (irreducible representations) have been tested to refine the magnetic structure of Ho_5Si_4. Those used in this work for the $Ho_5(Si_xGe_{1-x})_4$ system are described in Table VII.[26] The best correspondence between the calculated and the measured data have been obtained for Ho_5Si_4 using the magnetic space group $Pnm'a'$, in which the spins located in the 4*e* and 8*d* sites are arranged following the magnetic modes F_xG_z and $F_{Bx}A_{By}G_{Bz}$, respectively. Figure 3 displays the magnetic structures at 2 K. It corresponds to a slightly noncollinear FM structure with the magnetization oriented mainly along the *a* axis. The deviation from colinearity stems from a weak AFM coupling observed along the *c* axis on the 4*e*, and the *b* and *c* axis on the 8*d* sites, resulting in

TABLE I. Crystallographic parameters of Ho_5Si_4 as refined from D1A neutron diffraction data collected at $T=100$, 30, and 2 K. Space group, lattice parameters, unit-cell volume, fractional atomic coordinates, atomic displacement parameters (B) and reliability factors are indicated.

		100 K	30 K	2 K
Space group		*Pnma*	*Pnma*	*Pnma*
a (Å)		7.333(1)	7.3177(2)	7.3175(2)
b (Å)		14.441(2)	14.4206(4)	14.4176(4)
c (Å)		7.630(1)	7.6158(2)	7.6156(2)
φ (deg.)		90	90	90
V (Å^3)		808.0 (2)	803.67 (4)	803.44 (4)
Ho1 (4*c*):	*x*	0.3474(9)	0.3480(7)	0.3484(7)
	y	$\frac{1}{4}$	$\frac{1}{4}$	$\frac{1}{4}$
	z	0.988(9)	0.9893(5)	0.9905(4)
Ho2 (8*d*):	*x*	0.0225(5)	0.0228(4)	0.0235(4)
	y	0.0980(3)	0.0971(1)	0.0967(1)
	z	0.8166(6)	0.8173(4)	0.8186(4)
Ho3 (8*d*):	*x*	0.1793(6)	0.1805(4)	0.1805(4)
	y	0.1234(3)	0.1234(2)	0.1228(1)
	z	0.3218(5)	0.3217(3)	0.3217(3)
$B_{\text{Ho sites}}$ (Å^2)		0.53(6)	−0.20(5)	−0.32(5)
Si1 (4*c*):	*x*	0.975(2)	0.972(3)	0.971(3)
	y	$\frac{1}{4}$	$\frac{1}{4}$	$\frac{1}{4}$
	z	0.106(2)	0.104(3)	0.106(3)
Si2 (4*c*):	*x*	0.235(2)	0.235(3)	0.233(3)
	y	$\frac{1}{4}$	$\frac{1}{4}$	$\frac{1}{4}$
	z	0.625(2)	0.625(3)	0.634(3)
Si3 (8*d*):	*x*	0.151(2)	0.158(3)	0.154(3)
	y	0.9620(6)	0.9638(9)	0.962(1)
	z	0.530(1)	0.530(2)	0.532(2)
$B_{\text{Si sites}}$ (Å^2)		1.0(1)	0.8(2)	0.9(2)
R_p/R_{wp} (%)		2.0/2.4	3.0/3.8	3.4/4.2
R_{Bragg} (%)		6.64	4.55	4.07
R_{mag} (%)			3.9	3.8
χ^2		6.2	4.2	3.4

TABLE II. Magnetic moment components of Ho_5Si_4 at $T=30$ and 2 K.

	$\mu_x(\mu_B)$		$\mu_y(\mu_B)$		$\mu_z(\mu_B)$		$\mu(\mu_B)$	
	30 K	2 K	30 K	2 K	30 K	2 K	30 K	2 K
Ho1 (4*c*)	9.1(2)	8.8(2)	0	0	0.5(1)	1.0(1)	9.2(2)	8.9(2)
Ho2 (8*d*)	8.2(1)	8.3(1)	−3.07(9)	−4.05(8)	0.8(1)	0.6(1)	8.8(2)	9.3(2)
Ho3 (8*d*)	8.6(1)	9.1(1)	0.6(1)	0.27(8)	−1.1(1)	−0.3(2)	8.7(1)	9.1(1)

canting angles with respect to the *a* direction of $\theta_{Ho1} \cong 6°$, $\theta_{Ho2} \cong 26°$, and $\theta_{Ho3} \cong 1°$.

B. Ho_5Si_3Ge

As in the parent compound Ho_5Si_4 described in the previous section, the D1B neutron thermodiffractogram of Ho_5Si_3Ge shows no structural change on cooling down to the ordering temperature. The room temperature monoclinic $P112_1/a$ $Gd_5Si_2Ge_2$-type *M* phase covers the whole temperature range. To investigate in detail the magnetic contribution to the neutron scattering, a thermodiffractogram was recorded on D1B over the temperature range 4–60 K which is displayed in Figs. 4(a) and 4(b). In Fig. 4(a) one can clearly see the upcome of magnetic scattering below $T_C = 45$ K. Found mostly on top of low intensity nuclear reflections, this magnetic intensity is related to a FM-like ordering. As in Ho_5Si_4, a small amount of 1:1 impurity phase (~6.5 wt. %) has been observed, which becomes magnetic at about 23 K and adopts an incommensurate structure before becoming commensurate at about 16 K [see Fig. 4(a)]. Figure 4(b) represents the low-angle region of the thermodiffractogram not included in Fig. 4(a). At $T'_C \sim 16$ K there is a small indication of another magnetic transition with the appearance of a small broad peak at $2\theta \sim 11°$. At $T \sim 8$ K, this peak moves slightly towards lower angles into a position which corresponds to a second magnetic phase with propagation vector $\mathbf{k}=(0\ 0\ \frac{1}{4})$. The evolution of these peaks and the temperatures at which they emerge are more clearly illustrated in Fig. 4(c), where the integrated intensity of the main magnetic reflection for the propagation vector $\mathbf{k}=(0\ 0\ 0)$, the small broad peak and the commensurate $(0\ 0\ \frac{1}{4})$-type reflection are plotted as a function of temperature. In this picture, we can see that the intensity corresponding to the main magnetic phase reaches a maximum at about 16 K, the temperature at which the small broad peak appears at $2\theta \sim 11°$. Between 16 and about 8 K a small decrease is found for the main phase with the incommensurate phase increasing. The sudden rise of the intensity of the latter coincides with the shift in 2θ and the onset of the $(0\ 0\ \frac{1}{4})$ phase. Below 8 K, the magnetic reflections associated with both the main commensurate and the $(0\ 0\ \frac{1}{4})$ phases increase strongly.

D1A diffractograms taken at $T=300$, 60, 30, 12, and 8 K have been refined; two examples of these patterns and their fits are displayed in Fig. 5. The crystallographic parameters and the magnetic moments components extracted from the refinements are listed in Tables III and IV, respectively. As in the monoclinic compounds of the $Er_5(Si_xGe_{1-x})_4$ series,

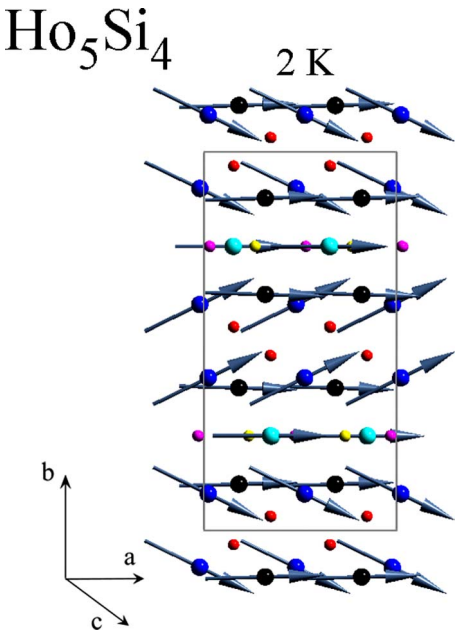

FIG. 3. (Color online) Spin arrangement in Ho_5Si_4 at $T=2$ K.

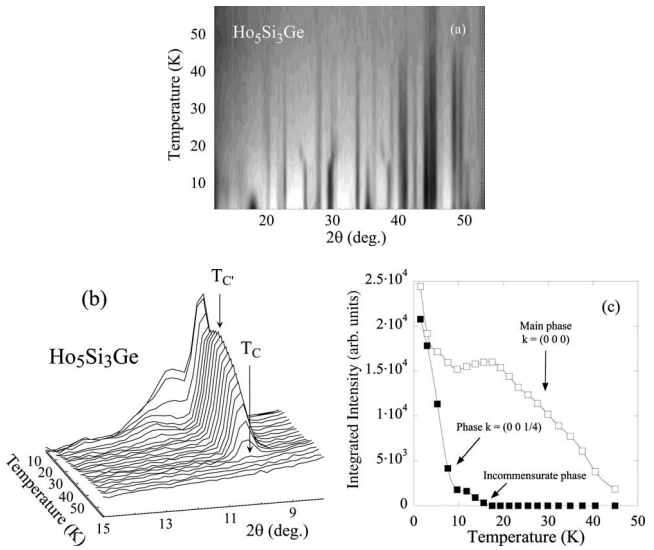

FIG. 4. (a) Contour plot of the neutron D1B thermodiffractogram of Ho_5Si_3Ge. (b) Detail of the low-angle region of panel a, where the magnetic transitions are indicated with arrows. (c) Integrated intensity of the peaks shown in panel b.

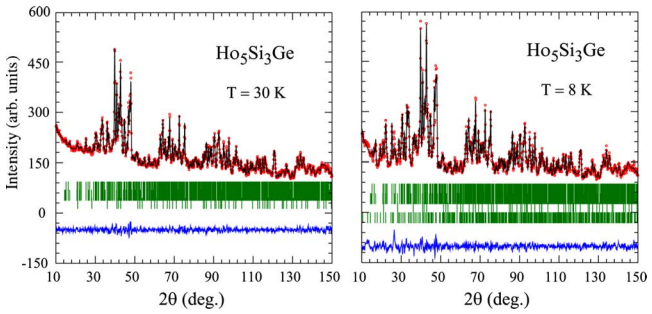

FIG. 5. (Color online) Neutron powder diffraction pattern of Ho_5Si_3Ge at $T=30$ K and 8 K collected in D1A diffractometer. The experiment (dots), the refinement (line) and their difference (line at the bottom) are represented. The vertical bars mark the reflections related to, from top to bottom, the main (structural) phase, the magnetic part of the main phase, the impurity (structural) phase, and the magnetic part of the impurity (absent at 30 K).

among the magnetic space group tested to refine the data (see Table VII), the best refinements of the magnetic part of the spectra at 30 and 8 K are obtained using the $P112_1'/a$ group with the magnetic modes $F_xF_yG_z$.[27] The magnetic structure at $T=30$ and 8 K of the main magnetic phase with $\mathbf{k}=(0\ 0\ 0)$ is illustrated in Fig. 6. The resulting spin arrangement is quite complex, but clear conclusions can be extracted. There is a strong FM coupling along the *a*-axis with an AFM canting along *c*. As in the erbium silicide and other monoclinic compounds of the 5:4 family, the magnetic moments located close to the existing interslab covalentlike Si(Ge)-Si(Ge) bonds (i.e. 2B and 3B positions) are larger than those placed near the unbonded pairs (2A and 3A) due to the strengthened FM coupling induced by bonding. Furthermore, the magnetic spins on sites close to the broken bonds tend to be mainly oriented within the *a*-*c* plane, i.e., the spins tend to be confined within the slab plane, whereas those located near the bonded pairs present a strong off-the-slab canting. Below the second magnetic transition T_C', the magnetic moment increases for all the Ho atoms, the differences between the magnetic moment values in the Ho2A and Ho3A compared to the other 3 Ho sites have decreased significantly (see Table IV).

The reason for refining the 8 K data and not the 2 K data resides in the possibility to exclude in the 8 K refinement the still weak magnetic peaks stemming from the second magnetic phase with $\mathbf{k}=(0\ 0\ \frac{1}{4})$. It was not possible to refine this second magnetic phase reliably from the 2 K data. The number of independent Ho spins increases in the four times bigger magnetic unit cell to 10. Assuming that this second magnetic phase is in concurrence to the main magnetic phase, an interpretation supported by the evolution of the magnetic peaks shown in Fig. 4(c), one can estimate the phase percentage of this second magnetic phase to about 25%. Although it seems reasonable to relate the two different magnetic phases to different portions (phase fractions) of the nuclear phase it is not possible to verify this due to the impossibility to resolve/separate the different nuclear phase fractions having identical or very similar lattice parameters. Testing the allowed irreducible representations for $\mathbf{k}=(0\ 0\ \frac{1}{4})$ a reasonably well fit of this minority magnetic phase can be achieved with an exclusively AFM structure seeing the spins directed along the a-direction. We have to recall here that this result is very approximate.

C. $Ho_5Si_2Ge_2$

The compound $Ho_5Si_2Ge_2$ crystallizes in the *Pnma* Sm_5Ge_4-type state [O(II)] at room temperature. No structural change has been observed when cooling down to 2 K. A larger amount of impurity phase 1:1 (about 13 wt. %) has been observed. On the other hand, no other 5:4 secondary phases have been detected, in agreement with the previous room temperature x-ray characterization.[20] The complexity of the magnetic structure of this compound at low temperature is illustrated by the contour plot of the D1B thermodiffractograms at low angles in the low-temperature range plotted in Fig. 7. The strongest magnetic peak found at $2\theta=10°$ has been excluded from this plot in order to allow the detailed view on the thermal behavior of the less intense magnetic peaks. In addition to an AFM ordering of the O(II) main phase with $\mathbf{k}=(0\ 0\ 0)$ at $T_N\sim 30$ K, the same 1:1 impurity already found in the two previously discussed members of the $Ho_5(Si_{1-x}Ge_x)_4$ series also orders AFM at about 26 K giving first rise to an incommensurate structure which becomes commensurate below 12 K. The 5:4 phase sees furthermore the appearance of two additional magnetic phases with the propagation vectors $\mathbf{k}=(0\ 0\ \frac{1}{4})$ as in the former Ho_5Si_3Ge compound, and $\mathbf{k}=(\frac{1}{2}\ 0\ 0)$. The phase with the propagation vector $\mathbf{k}=(0\ 0\ \frac{1}{4})$ emerges at about 15 K, whereas the phase with $\mathbf{k}=(\frac{1}{2}\ 0\ 0)$ starts to grow at about 12 K. The broad second magnetic transition found by Thuy *et al.*[19] on a similar $Ho_5Si_2Ge_2$ compound at about 15 K must be related either to the onset of the magnetic phases with $\mathbf{k}=(0\ 0\ \frac{1}{4})$ and/or $\mathbf{k}=(\frac{1}{2}\ 0\ 0)$ stemming from the 5:4 phase or to the 1:1 impurity phase, the nuclear Bragg peaks of which are clearly visible in the x-ray data shown in Fig. 1 of Ref. 19. Due to the similarity in the ordering temperatures between the main and the impurity phases, there is a lack of high resolution diffraction patterns with the 5:4 phase magnetically ordered as one whole phase and the impurity phase still in the PM state. The coexistence of three magnetic phases in the 5:4 phase together with the presence of the 1:1 magnetic impurity phase makes a complete refinement of the magnetic structures found in $Ho_5Si_2Ge_2$ at low temperatures not possible. However, as a first approach to the solution of the magnetic structure stemming from the main magnetic phase with $\mathbf{k}=(0\ 0\ 0)$, we have fitted the high resolution data collected at 2 K excluding from the calculation most of the magnetic peaks deriving from the two additional magnetic phases of the 5:4 compound. Though this fit cannot be taken into account quantitatively, the best refinement was clearly obtained assuming the magnetic space group $Pn'm'a'$, see Table VII. This result is reasonable taking into account that the same magnetic symmetry will be found afterward in another member of the family with the same crystal structure, Ho_5Ge_4, at temperatures just below T_N.

D. Ho_5Ge_4

The compound Ho_5Ge_4, which at room temperature crystallizes in the well known O(II) structure (*Pnma*

TABLE III. Crystallographic parameters of Ho_5Si_3Ge as refined from D1A neutron diffraction data collected at $T=300$, 60, 30, 12, 8, and 2 K. Space group, lattice parameters, unit-cell volume, fractional atomic coordinates, atomic displacement parameters (B) and reliability factors are indicated. $M=0.75$ Si +0.25 Ge.

		300 K	60 K	30 K	12 K	8 K
Space group		$P112_1/a$	$P112_1/a$	$P112_1/a$	$P112_1/a$	$P112_1/a$
a (Å)		7.4258(3)	7.4150(3)	7.4143(4)	7.4147(3)	7.4127(4)
b (Å)		14.5016(6)	14.4648(6)	14.4640(6)	14.4685(5)	14.4666(7)
c (Å)		7.6243(4)	7.6070(4)	7.6063(3)	7.6069(3)	7.6053(4)
φ (deg.)		93.002(4)	93.204(3)	93.262(4)	93.303(3)	93.312(3)
V (Å^3)		819.90(6)	814.63(6)	814.39(6)	814.71(5)	814.21(8)
Ho1 (4*e*):	*x*	0.324(2)	0.325(1)	0.325(1)	0.325(1)	0.325(2)
	y	0.2467(5)	0.2471(5)	0.2474(5)	0.2475(4)	0.2473(5)
	z	0.0056(9)	0.008(1)	0.005(1)	0.0041(7)	0.007(1)
Ho2A (4*e*):	*x*	−0.010(1)	−0.009(1)	−0.010(1)	−0.008(1)	−0.008(1)
	y	0.0995(5)	0.0987(5)	0.0997(6)	0.0995(4)	0.1009(6)
	z	0.178(1)	0.180(1)	0.181(1)	0.181(1)	0.177(1)
Ho2B (4*e*):	*x*	0.013(1)	0.017(1)	0.0172(9)	0.0174(8)	0.016(1)
	y	0.4019(5)	0.4020(5)	0.4018(4)	0.4013(3)	0.4024(5)
	z	0.182(1)	0.180(1)	0.1812(9)	0.1802(7)	0.182(1)
Ho3A (4*e*):	*x*	0.359(1)	0.3593(9)	0.361(1)	0.358(1)	0.358(1)
	y	0.8810(5)	0.8798(5)	0.8806(5)	0.8798(5)	0.8821(6)
	z	0.168(1)	0.164(1)	0.165(1)	0.168(1)	0.165(1)
Ho3B (4*e*):	*x*	0.333(1)	0.333(1)	0.330(1)	0.3305(9)	0.332(1)
	y	0.6227(4)	0.6236(5)	0.6235(4)	0.6226(3)	0.6226(4)
	z	0.177(1)	0.176(1)	0.1762(9)	0.1786(7)	0.175(1)
$B_{\text{Ho sites}}$ (Å^2)		0.51(6)	0.30(7)	0.04(7)	0.09(6)	0.23(8)
M1 (4*e*):	*x*	0.956(2)	0.953(2)	0.957(2)	0.950(2)	0.956(3)
	y	0.2504(8)	0.2518(9)	0.252(1)	0.250(1)	0.252(2)
	z	0.895(1)	0.891(1)	0.889 (2)	0.895 (2)	0.893(3)
M2 (4*e*):	*x*	0.208(2)	0.204(2)	0.210(2)	0.208(2)	0.211(3)
	y	0.2527(7)	0.2524(7)	0.252(9)	0.252(9)	0.249(1)
	z	0.366(1)	0.366(1)	0.366(2)	0.367(2)	0.367(3)
M3A (4*e*):	*x*	0.209(2)	0.209(2)	0.206(2)	0.205(2)	0.207(3)
	y	0.9596(7)	0.9596(7)	0.956(1)	0.956(1)	0.954(2)
	z	0.471(2)	0.471(2)	0.466(2)	0.467(2)	0.464(3)
M3B (4*e*):	*x*	0.158(2)	0.153(2)	0.152(2)	0.151(2)	0.151(3)
	y	0.5398(8)	0.5393(8)	0.540(1)	0.540(1)	0.538(1)
	z	0.465 (1)	0.469 (2)	0.471(2)	0.470(2)	0.474(3)
$B_{M\ \text{sites}}$ (Å^2)		0.57	0.57	0.57	0.57	0.57
R_p/R_{wp} (%)		1.5/1.9	1.8/2.2	2.2/2.9	2.0/2.6	3.3/4.1
R_{Bragg} (%)		4.5	5.0	3.5	2.8	3.6
R_{mag} (%)				5.0	4.0	4.6
χ^2		2.2	2.0	2.6	6.2	3.4

TABLE IV. Magnetic moment components of the $\mathbf{k}=(0\ 0\ 0)$ magnetic phase of Ho_5Si_3Ge at $T=30$, 12, and 8 K.

4*e* site		Ho1	Ho2A	Ho2B	Ho3A	Ho3B
$\mu_x(\mu_B)$	30 K	3.7(2)	1.4(1)	5.3(2)	1.0(2)	3.7(2)
	12 K	6.5(1)	2.9(1)	6.6(1)	3.5(1)	6.4(1)
	8 K	6.3(2)	3.4(1)	7.4(2)	3.5(1)	6.8(2)
$\mu_y(\mu_B)$	30 K	1.1(2)	−0.0(2)	5.0(2)	0.7(2)	3.0(2)
	12 K	0.4(1)	−0.4(2)	5.2(1)	−0.5(2)	0.5(1)
	8 K	−1.0(2)	−0.4(2)	4.1(2)	−1.2(2)	−0.2(2)
$\mu_z(\mu_B)$	30 K	1.0(2)	−0.0(2)	1.5(2)	−0.3(3)	−0.2(2)
	12 K	−0.1(1)	−3.2(1)	1.4(1)	−0.7(2)	−1.4(1)
	8K	−1.0(2)	−3.9(2)	1.9(2)	−2.2(2)	−1.2(2)
$\mu(\mu_B)$	30 K	3.9(2)	1.4(2)	7.2(1)	1.2(2)	4.6(1)
	12 K	6.5(1)	4.4(1)	8.3(1)	3.6(1)	6.5(1)
	8 K	6.5(2)	5.1(2)	8.4(2)	4.4(2)	6.9(2)

Sm_5Ge_4-type), remains in the same crystallographic state when cooling down to the AFM ordering temperature of $T_N \sim 30$ K. No secondary phases have been found in the PM regime. This is supported by refinements of D1A diffraction patterns at 300 and 50 K shown in Table V together with the results of further Rietveld analysis at 25, 20, and 2 K also listed there. A low-temperature D1B thermodiffractogram contour plot is pictured in Fig. 8(a) to illustrate the evolution of the low-temperature magnetic state. In this image we can see that, in addition to the AFM ordering transition with $\mathbf{k}=(0\ 0\ 0)$, there is a second set of magnetic peaks appearing at about 17 K, in agreement with the results of Schobinger and Niggli.[21] As explained below, the second set of magnetic reflections has to be indexed with a second propagation vector $\mathbf{k}=(0\ 0\ \frac{1}{2})$ acting in fact on the same nuclear phase.

In order to clarify the relation between the two magnetic phases existing at low temperature, we have plotted in Fig. 8(b) the integrated intensity of the two strongest magnetic Bragg peaks (0 1 0) and $(0\ 1\ \frac{1}{2})$ which stand for the $\mathbf{k}=(0\ 0\ 0)$ and the $\mathbf{k}=(0\ 0\ \frac{1}{2})$ type magnetic structures, respectively. The first magnetic transition sets in at about 30 K and accelerates strongly below 25 K. The second magnetic structure first appears at about 17 K concomitant with a slight decrease of the (0 1 0) magnetic Bragg peak of the first magnetic structure.

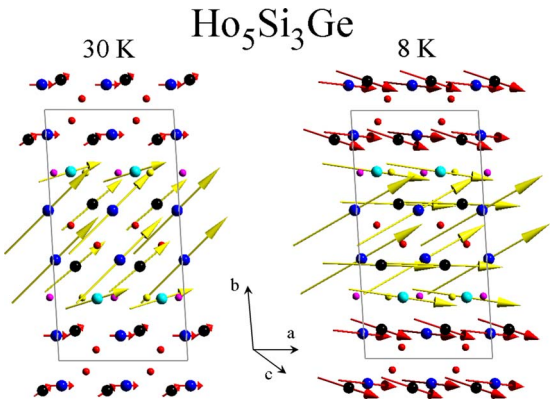

FIG. 6. (Color online) Spin arrangement in Ho_5Si_3Ge at $T=30$ K and $T=8$ K.

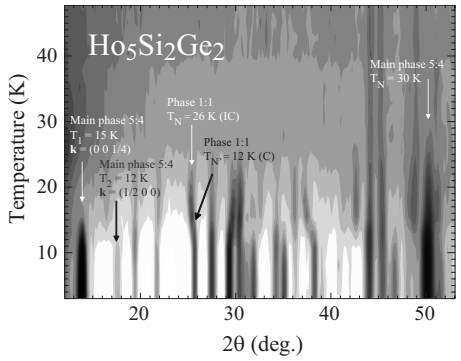

FIG. 7. Contour plot of the neutron D1B thermodiffractogram of $Ho_5Si_2Ge_2$. The reflections representing the different magnetic phases are marked with arrows. In the case of the impurity, the low-temperature magnetic states are labeled as commensurate (C) or incommensurate (IC). The strongest magnetic peak at $2\theta=10°$ is not shown here to allow a better visibility of the details of the different phase transitions.

The D1A diffraction pattern collected at 25 K already shows a magnetically ordered state. The best refinement of the magnetic structure has been obtained using the magnetic space group $Pn'm'a'$ listed in Table VII, in agreement to the findings of Schobinger and Niggli.[21] The magnetic moments at 25 K are still very low due to the proximity of the Néel temperature, see Table VI.

A strong change in the appearance of the diffraction patterns happens between 25 and 20 K: some of the nuclear peaks get significantly broadened while others remain sharp indicating a strong anisotropic microstructural strain in the $(h\ 0\ l)$ direction. The recently published paper by Singh *et al.*[21] gave us the needed additional information to interpret this effect, i.e., Ho_5Ge_4 undergoes a first-order structural transformation in this range of temperatures and adopts in fact a new monoclinic $P2_1/m$ structure type below 23 K apparently concomitant with the onset of the AFM state. The structural transition from *Pnma* to $P2_1/m$ is, as already mentioned by Singh *et al.*,[21] only accompanied by a small change of the lattice parameters, i.e. $\Delta a/a \cong -0.05\%$, $\Delta b/b \cong -0.06\%$, $\Delta c/c \cong 0.1\%$ (see Table VI). Due to the strong dominance of magnetic scattering at low temperatures, the subtle changes in the nuclear scattering in the nuclear scattering when going from *Pnma* to $P2_1/m$ are nearly not visible in neutron diffraction. Figure 9 shows a 2θ region where the splitting of the (4 5 4) Bragg reflection of the orthorhombic *Pnma* phase into the (−4 5 4) and the (4 5 4) reflections of the monoclinic $P2_1/m$ phase is visible when going from 25 down to 20 K. The same plot shows also that, although already in the magnetic state, no sign of the splitting is visible at 25 K in comparison to the 50 K data set. It must be concluded that with decreasing temperature the increasing AFM arrangement of magnetic moments cannot longer be accommodated in the orthorhombic O(II) *Pnma* structure and leads over strong anisotropic strain to the structural transition to monoclinic $P2_1/m$ as described by Singh *et al.* Furthermore, our study demonstrates that the magnetic and

TABLE V. Crystallographic parameters of Ho_5Ge_4 refined from D1A data collected at $T=300$, 50, and 25 K, and from D2B at $T=20$ and 2 K. Space group, lattice parameters, unit-cell volume, fractional atomic coordinates, atomic displacement parameters (B) and reliability factors are indicated. The B factors without error values have been fixed.

		300 K	50 K	25 K			20 K	2 K
Space group		*Pnma*	*Pnma*	*Pnma*			$P2_1/m$	$P2_1/m$
a (Å)		7.5841(4)	7.5669(3)	7.5631(4)			7.559(1)	7.5584(8)
b (Å)		14.5968(7)	14.5574(6)	14.5526(6)			14.544(1)	14.546(1)
c (Å)		7.6541(4)	7.6300(4)	7.6228(4)			7.614(9)	7.6141(8)
β (deg.)		90	90	90			90.55(1)	90.599(8)
V (Å^3)		847.34(7)	840.48(6)	839.00(7)			837.0(2)	837.1(2)
Ho1 (4*c*)	x	0.287(1)	0.287(1)	0.288(1)	Ho1A (2*e*)	x	0.208(5)	0.209(5)
	y	$\frac{1}{4}$	$\frac{1}{4}$	$\frac{1}{4}$		y	$\frac{1}{4}$	$\frac{1}{4}$
	z	−0.001(1)	−0.001(1)	0.999 (1)		z	0.490(5)	0.493(5)
					Ho1B (2*e*)	x	0.703(5)	0.718(5)
						y	$\frac{1}{4}$	$\frac{1}{4}$
						z	−0.009(5)	−0.0007(5)
Ho2 (8*d*)	x	−0.0272(7)	−0.0296(6)	−0.0296(7)	Ho2A (4*f*)	x	−0.040(3)	−0.041(3)
	y	0.1000(3)	0.1008(3)	0.1003(3)		y	0.600(1)	0.601(1)
	z	0.1785(8)	0.1788(7)	0.1792(8)		z	0.177(3)	0.172(3)
					Ho2B (4*f*)	x	0.470(4)	0.465(3)
						y	0.600(1)	0.602(1)
						z	0.177(3)	0.322(2)
Ho3 (8*d*)	x	0.3783(7)	0.3810 (7)	0.3816(8)	Ho3A (4*f*)	x	0.384(3)	0.387(3)
	y	0.8833(4)	0.8833(3)	0.8831(3)		y	0.114(1)	0.113(1)
	z	0.1597(8)	0.1596(8)	0.1598 (8)		z	0.163(3)	0.169(3)
					Ho3B (4*f*)	x	0.883(4)	0.882(2)
						y	0.116(2)	0.1180(9)
						z	0.339(3)	0.333(2)
$B_{\text{Ho sites}}$ (Å^2)		1.04(8)	0.61(7)	0.2			0.2	0.2
Ge1 (4*c*)	x	0.920(1)	0.918(1)	0.919 (1)	Ge1A (2*e*)	x	0.840(5)	0.834(5)
	y	$\frac{1}{4}$	$\frac{1}{4}$	$\frac{1}{4}$		y	$\frac{1}{4}$	$\frac{1}{4}$
	z	0.884(1)	0.886(1)	0.885(1)		z	−0.365(4)	−0.362(4)
					Ge1B (2*e*)	x	0.315(4)	0.324(5)
						y	$\frac{1}{4}$	$\frac{1}{4}$
						z	0.859(4)	0.865(4)
Ge2 (4*c*)	x	0.167(1)	0.165(1)	0.166(1)	Ge2A (2*e*)	x	0.066(5)	0.065(5)
	y	$\frac{1}{4}$	$\frac{1}{4}$	$\frac{1}{4}$		y	$\frac{1}{4}$	$\frac{1}{4}$
	z	0.362(1)	0.362(1)	0.365(1)		z	0.124(5)	0.124(5)
					Ge2B (2*e*)	x	0.586(5)	0.586(5)
						y	$\frac{1}{4}$	$\frac{1}{4}$
						z	0.400(5)	0.391(5)
Ge3 (8*d*)	x	0.2178(9)	0.2190(8)	0.2194(8)	Ge3A (4*f*)	x	0.230(3)	0.226(3)
	y	0.9560(4)	0.9565(4)	0.9570 (4)		y	0.049(2)	0.049(2)
	z	0.4688(8)	0.4703(8)	0.4693(8)		z	0.463(3)	0.457(3)
					Ge3B (4*f*)	x	0.723(3)	0.722(3)
						y	0.036(2)	0.039(2)
						z	0.024(3)	0.026(3)
$B_{\text{Ge sites}}$ (Å^2)		1.28(8)	0.93(8)	0.2			0.2	0.2
R_p/R_{wp} (%)		1.9/2.5	2.2/2.8	2.3/3.0			4.4/6.1	4.9/6.3
R_{Bragg} (%)		8.0	8.0	7.9			7.1	6.7
R_{mag} (%)				13.8			8.7	6.2–8.0
χ^2		2.9	2.5	2.7			7.8	5.3

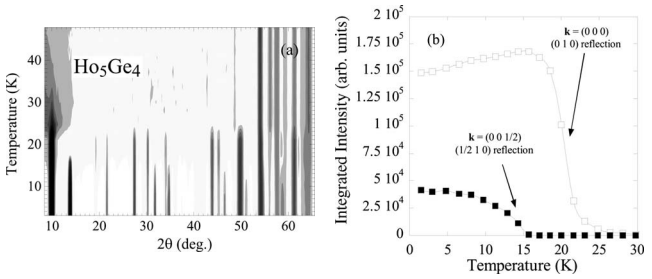

FIG. 8. (a) Contour plot of the neutron D1B thermodiffractogram of Ho_5Ge_4. (b) Integrated intensity of the main peaks of the two different propagation vectors.

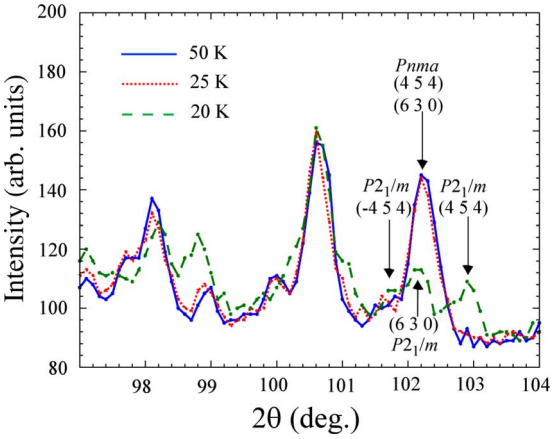

FIG. 9. (Color online) Comparison of the neutron diffractograms of Ho_5Ge_4 at $T=50$, 25, and 20 K in an angular region where the onset of the $P2_1/m$ phase can be observed.

structural transitions are decoupled by ~5 K. A similar situation was found in $Tb_5Si_2Ge_2$ where the M-O(I) structural transition takes place about 10 K below the $T_C=120$ K and only the application of an external hydrostatic pressure reforms the coupling.[5] In Er_5Si_4 the effect is even noticeable; the structural transition does not occur at low temperature, and the increasing pressure enables the onset and subsequent recoupling of the magnetic and structural transformations.[15] Thus, the case of decoupled magnetic and structure transitions seems to predominate when magnetic anisotropic is significantly strong, in sharp contrast with the Gd-based compounds.[6] The strong increase of the magnetic (0 1 0) reflection below about 23 K [see Fig. 8(b)] reflects the no longer hindered development of the AFM structure. In this context, one has to question whether the low-temperature nuclear structure of $Ho_5Ge_2Si_2$ really stays O(II) or the appearance of the second propagation vector–indexed as $(\frac{1}{2}\ 0\ 0)$ in the *Pnma* setting–indicates a situation similar to Ho_5Ge_4 with a structural transition to $P2_1/m$. However, a detailed inspection of the regions of the neutron diffraction data which are the most sensitive to a possible change from

TABLE VI. Magnetic moments of the magnetic phases of Ho_5Ge_4 at $T=25$, 20 and 2 K.

	$\mathbf{k_1}=(0\ 0\ 0)$			
$T=25$ K$-Pnma$	$\mu_x(\mu_B)$	$\mu_y(\mu_B)$	$\mu_z(\mu_B)$	$\mu(\mu_B)$
Ho1 (4*c*)	1.5(3)	0	0.2(8)	1.5(3)
Ho2 (8*d*)	0.3(2)	−0.6(3)	1.0(2)	1.2(2)
Ho3 (8*d*)	−1.3(2)	0	−0.4(4)	1.4(2)
$T=20$ K$-P2_1/m$	$\mathbf{k_1}=(0\ 0\ 0)$			
	$\mu_x(\mu_B)$	$\mu_y(\mu_B)$	$\mu_z(\mu_B)$	$\mu(\mu_B)$
Ho1A (2*e*)	−5.5(2)		0	5.5(2)
Ho1B (2*e*)	−5.5(2)		0	5.5(2)
Ho2A (4*f*)	6.3(2)		−4.6(2)	7.8(3)
Ho2B (4*f*)	0		0	0
Ho3A (4*f*)	6.3(2)		−4.6(2)	7.8(3)
Ho3B (4*f*)	0		0	0

$T=2$ K$-P2_1/m$	$\mathbf{k_1}=(0\ 0\ 0)$,			$\mathbf{k_2}=(0\ 0\ \frac{1}{2})$			
	$\mu_x(\mu_B)$	$\mu_y(\mu_B)$	$\mu_z(\mu_B)$	$\mu_x(\mu_B)$	$\mu_y(\mu_B)$	$\mu_z(\mu_B)$	$\mu(\mu_B)$
Ho1A (2*e*)	−4.4(2)		0	0		−6.1(3)	7.5(3)
Ho1B (2*e*)	−7.7(2)		0	0		0	7.7(3)
Ho2A (4*f*)	6.3(2)		−5.5(2)	0		0	8.4(3)
Ho2B (4*f*)	0		0	6.3(2)		5.5(2)	8.4(3)
Ho3A (4*f*)	−6.3(2)		5.5(2)	0		0	8.4(3)
Ho3B (4*f*)			0	−6.3(2)		−5.5	8.4(3)

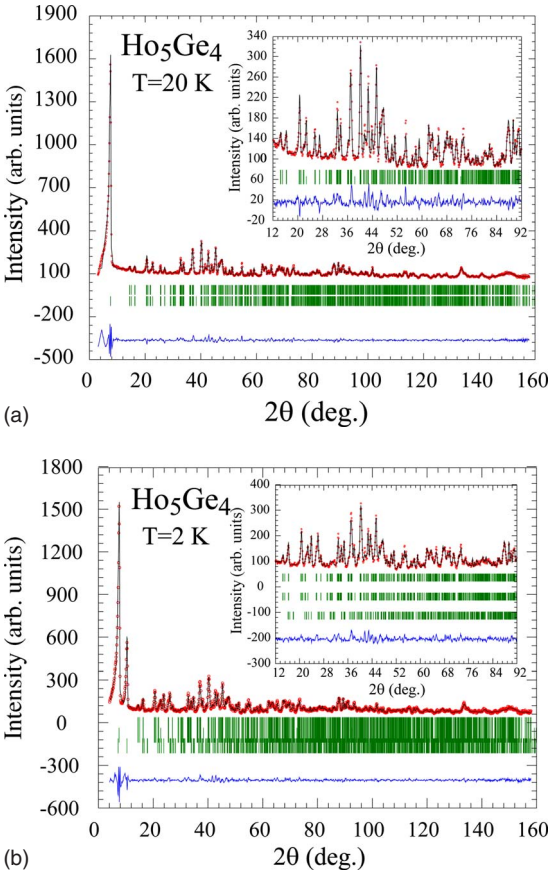

FIG. 10. (Color online) Neutron powder diffraction pattern of Ho_5Ge_4 at $T=20$ and 2 K collected on D1A. The insets show the same spectra excluding the high intensity low-angle magnetic reflections. The experiment (dots), the refinement (line) and their difference (line at the bottom) are represented. The vertical bars mark the reflections related to, from top to bottom: the structural phase and the magnetic part of the main phase at 20 K; the structural phase, the magnetic part with $\mathbf{k}=(0\ 0\ 0)$ and the magnetic part with $\mathbf{k}=(0\ 0\ \frac{1}{2})$ at 2 K.

Pnma to $P2_1/m$ did not show any broadening or change on cooling from 60 K over 16 K down to 2 K, which is consistent with the absence of any thermal expansion anomaly.[20]

To refine the magnetic structure of Ho_5Ge_4 one has to take into account that when going from *Pnma* to $P2_1/m$ the three independent Ho sites of *Pnma* (two 8*d* and one 4*c* site) split into six independent Ho sites in $P2_1/m$ (four 4*f* and two 2*e* sites). Symmetry analysis shows the presence of four allowed irreducible representations for the propagation vector $\mathbf{k}=(0\ 0\ 0)$ in $P2_1/m$. The magnetic structure adopted by Ho_5Ge_4 at 20 K [see pattern in Fig. 10(a)] follows the representation 2 describing a $A_xC_yA_z$ coupling between the four Ho spins of every independent 4f site and an AFM coupling in *x* and *z* direction between the 2 Ho spins of each of the independent 2*e* sites. This corresponds to the magnetic space group $P2_1/m'$ (see Table VII). The allowed *y* component of the Ho spins on the 4*f* sites refines to zero, so the magnetic moments are confined in the *ac* plane, which actually corresponds with the plane of the monoclinic distortion. The refinement reveals that a new coupling linking the sites Ho2A and Ho3A is present in the adopted magnetic structure (see Table VI). A strong anisotropy in the magnetic couplings is, however, reflected in the fact that two out of the six independent Ho sites (Ho2B and Ho3B) are not carrying any magnetic moment. The summary of the refinement at 25 K results are listed in Table V (the structural data) and in Table VI (the determined magnetic moment components). Figure 11 displays the magnetic structure where the non magnetic Ho atoms form non magnetic layers in the *ab* plane.

The new magnetic state arising at about 18 K sees the appearance of a second propagation vector $\mathbf{k}=(0\ 0\ \frac{1}{2})$ within the $P2_1/m$ structure. Symmetry analysis shows that the same irreducible representations are present for both propagation vectors $\mathbf{k}_1=(0\ 0\ 0)$ and $\mathbf{k}_2=(0\ 0\ \frac{1}{2})$. Refining the high resolution data at 2 K, it turns out that the formerly nonmagnetic Ho sites are those sites onto which the second propagation vector acts mainly. The coupling is here, however, described by the irreducible representation three, $F_xG_yF_z$ for the 4*f* site and F_xF_z for the 2*e* site. This leads—as the *y* component refines to zero—through the action of the propagation vector $\mathbf{k}_2=(0\ 0\ \frac{1}{2})$ again to a purely AFM structure in a doubled magnetic unit cell in the *c* direction. The refinement of the neutron data at 2 K is shown in Fig. 10(b) and the resulting magnetic structure is drawn in Fig. 11. The comprehensive structural data at 2 K are included in Table V and the magnetic moment components in Table VI. As the refinement showed that the moment values of the Ho sites 2A and 3A and those of the Ho sites 2B and 3B can be coupled without affecting the goodness of the fit, the magnetic structure turns out to be fairly simple. Magnetic spins in Fig. 11 shown in green (Ho sites 2A, 3A and 1B) are only following the propagation vector $\mathbf{k}_1=(0\ 0\ 0)$, whereas those in red (Ho sites 2B and 3B) are governed exclusively by $\mathbf{k}_2=(0\ 0\ \frac{1}{2})$ while only the spins of the Ho site 1A shown in yellow are determined by the combination of both propagation vectors: While $\mathbf{k}_1=(0\ 0\ 0)$ acts on the *x* component of Ho1A, its *z* component follows $\mathbf{k}_2=(0\ 0\ \frac{1}{2})$. The simplicity of the adopted low-temperature magnetic structure is mirrored as well in the very similar magnetic moment values of the different Ho sites, varying between $7.7(3)\mu_B$ and $8.4(3)\mu_B$. As already observed at 20 K, the magnetic moments are restricted to the *ac* plane. We want to remark that the observation of the strong anisotropic strain between 25 and 20 K mirrors a distribution of *a* and *c* lattice parameters preceding the crystallographic transformation. This distribution of *a* and *c* lattice parameters seems to be triggered by the upcoming magnetism and corresponds to a correlation between the spin ordering within the *a*-*c* plane and the monoclinic distortion that stabilizes the $P2_1/m$ phase.

E. Ho_5Ge_4 under magnetic field

Neutron experiments have been performed in applied magnetic field in D2B to determine the magnetic-field dependence of the structural and magnetic state of Ho_5Ge_4. Due to a slight reorientation of the polycrystalline grains of the powder—which had been compacted in the vanadium sample container—under the effect of the magnetic field, it was not possible to analyse the data quantitatively. The induced reorientation remained, however, present even after

TABLE VII. Sign convention of the four permitted magnetic modes for the nonequivalent symmetry positions 4*e* in the $P112_1/a$ space group with the magnetic propagation vector $\mathbf{k}=(0\ 0\ 0)$, for the 4*c* and 8*d* in the $Pnm'a'$ and $Pn'm'a'$ magnetic space groups in the *Pnma* space group (taken from Ref. 26 and 27), and for the 4*f* and 2*e* positions in the $P2_1/m$ space group.

				Magnetic space group			
		Position		$P112_1/a$	$P112_1/a'$	$P112_1'/a$	$P112_1'/a'$
i		4*e*		$C_xC_yA_z$	$G_xG_yF_z$	$F_xF_yG_z$	$A_xA_yC_z$
1	x	y	z	+++	+++	+++	+++
2	$\frac{1}{2}-x$	$-y$	$\frac{1}{2}+z$	++−	−−+	++−	−−+
3	$-x$	$-y$	$-z$	−−−	+++	+++	−−−
4	$\frac{1}{2}+x$	y	$\frac{1}{2}-z$	−−+	−−+	++−	++−
		Position		$Pnm'a'$		$Pn'm'a'$	
i		8*d*		$F_{Bx}A_{By}G_{Bz}$		$R_xQ_yL_z$	
1	x	y	z	+++		+++	
2	$\frac{1}{2}+x$	$\frac{1}{2}-y$	$\frac{1}{2}-z$	+−−		+−−	
3	$-x$	$\frac{1}{2}+y$	$-z$	+−+		−+−	
4	$\frac{1}{2}-x$	$-y$	$\frac{1}{2}+z$	++−		−−+	
5	$-x$	$-y$	$-z$	+++		−−−	
6	$\frac{1}{2}-x$	$\frac{1}{2}+y$	$\frac{1}{2}+z$	+−−		−++	
7	x	$\frac{1}{2}-y$	z	+−+		+−+	
8	$\frac{1}{2}+x$	y	$\frac{1}{2}-z$	++−		++−	
i		4*c*		F_xG_z		A_xG_z	
1	x	$\frac{1}{4}$	z	+ +		+ +	
2	$-x$	$\frac{3}{4}$	$-z$	+ +		− −	
3	$\frac{1}{2}-x$	$\frac{3}{4}$	$\frac{1}{2}+z$	+ −		− +	
4	$\frac{1}{2}+x$	$\frac{1}{4}$	$\frac{1}{2}-z$	+ −		+ −	
		Position		$P2_1/m$	$P2_1/m'$	$P2_1'/m'$	$P2_1'/m$
i		4*f*		$G_xF_yG_z$	$A_xC_yA_z$	$F_xG_yF_z$	$C_xA_yC_z$
1	x	y	z	+++	+++	+++	+++
2	$-x$	$y+\frac{1}{2}$	$-z$	−+−	−+−	+−+	+−+
3	$-x$	$-y$	$-z$	+++	−−−	+++	−−−
4	x	$-y+\frac{1}{2}$	z	−+−	+−+	+−+	−+−
i		2*e*		F_y	AF_xAF_Z	F_xF_Z	AF_y
1	x	y	z	+	+ +	+ +	+
2	$-x$	$\frac{3}{4}$	$-z$	+	− −	+ +	−

removing the magnetic field. The zero field data presented in Fig. 12 were taken after a first passage to 6 T and are affected by the same reorientation effect as the 6 T data allowing thereby the direct comparison of the Bragg peak intensities and the visualization of the upcoming ferromagnetism.

At low temperature, a ferromagnetic state is induced in Ho_5Ge_4 by the application of a magnetic field. This can be observed in Fig. 12, where the D2B diffractograms collected at 5 K at zero field and 6 T are depicted. The inset shows a detail of a particular angular range where the generalized increase of the magnetic signal in the Bragg positions is more evident. This phenomenon is in agreement with the macroscopic magnetization measurements, where an abrupt change in the magnetization is found at ~1.5 T.[20]

Singh *et al.* have reported that the application of a magnetic field induces the reformation of an O(II) crystal phase in coexistence with the low field $P2_1/m$ [up to 30% of O(II) phase at 3.5 T]. Although we cannot extract quantitative results on the crystal structure or phase coexistence from our neutron data, our experiments point toward a close relationship between the crystal phases and the magnetic structures. More precisely, we have found the different influence of the magnetic field in the two magnetic couplings, $\mathbf{k}=(0\ 0\ 0)$ and $\mathbf{k}=(0\ 0\ \frac{1}{2})$, present at low temperature. This is illustrated in Fig. 13(a), where the effect of the magnetic field on the two main magnetic peaks coming from the $\mathbf{k}=(0\ 0\ 0)$ and the $\mathbf{k}=(0\ 0\ \frac{1}{2})$ propagation vectors of the AFM state at 5 K are shown. The difference in the effect of the magnetic field is remarkable. While the magnetic field leads to a very fast decline of the magnetic peak associated to the $\mathbf{k}=(0\ 0\ 0)$ propagation vector, the $\mathbf{k}=(0\ 0\ \frac{1}{2})$ type magnetic peak remains still strongly present at 6 T. Figure 13(b) dis-

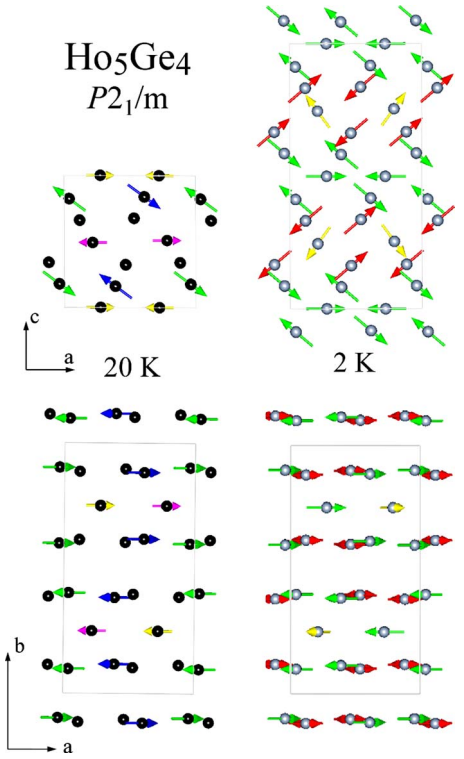

FIG. 11. (Color online) Spin arrangement of the two phases refined in Ho_5Ge_4 at $T=20$ and 2 K.

plays the integrated normalized intensities of these peaks as a function of the magnetic field at 5 K as well as the field dependence of the $\mathbf{k}=(0\ 0\ 0)$ type peak at 20 and 25 K. It becomes clear that at 20 K all AFM has already gone at H >3 T.

Looking at Fig. 13(b) one could conclude that it is the $\mathbf{k}=(0\ 0\ \frac{1}{2})$ phase that is closely related to the change from O(II) to monoclinic, as there is still about 25% decrease of the $\mathbf{k}=(0\ 0\ \frac{1}{2})$ signal under 3 T and about 60% under 6 T at 5 K. Singh *et al.* reports that only 30% of O(II) *Pnma* phase is left at 15 K and 3.5 T, which is compatible with our estimation. On the other hand, the transition from *Pnma* to $P21/m$ has already happened at 20 K on cooling, where no

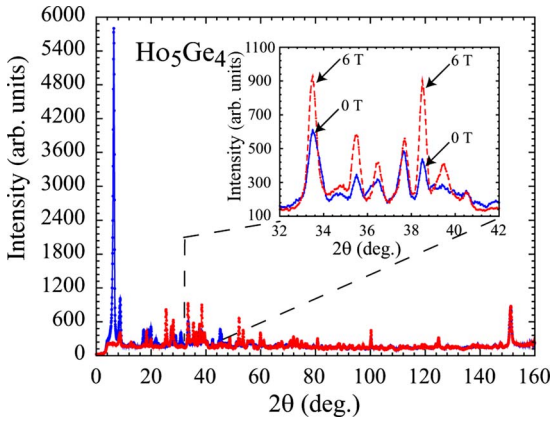

FIG. 12. (Color online) Comparison of the D2B diffractogram of Ho_5Ge_4 at zero field and at maximum applied magnetic field (6 T). The inset illustrates the formation of a ferromagnetic state at 6 T.

sign of the $\mathbf{k}=(0\ 0\ \frac{1}{2})$ magnetic state exists yet. Taking into account the complexity of the low-temperature Ho_5Ge_4 state and the difficulties to do a quantitative study by neutron diffraction in this compound in polycrystalline state, the growth of high quality single crystals will be decisive to accurately unveil the relationship between the structure and the magnetic ordering in this compound.

IV. CONCLUSIONS

We have performed a microscopic characterization of polycrystalline samples of selected compositions ($x=1$, 0.75, 0.5 and 0) with different room temperature crystallographic structures of the magnetocaloric compound $Ho_5(Si_xGe_{1-x})_4$ by means of neutron powder diffraction as a function of temperature. The results of this investigation has given rise to a new magnetic-crystallographic phase diagram represented in Fig. 14, where the low-temperature crystal and magnetic structures determined from neutron diffraction experiments are summarized.

The alloys with compositions $x=1$, 0.75, and 0.5 preserve their room-temperature crystallographic phases when cooling

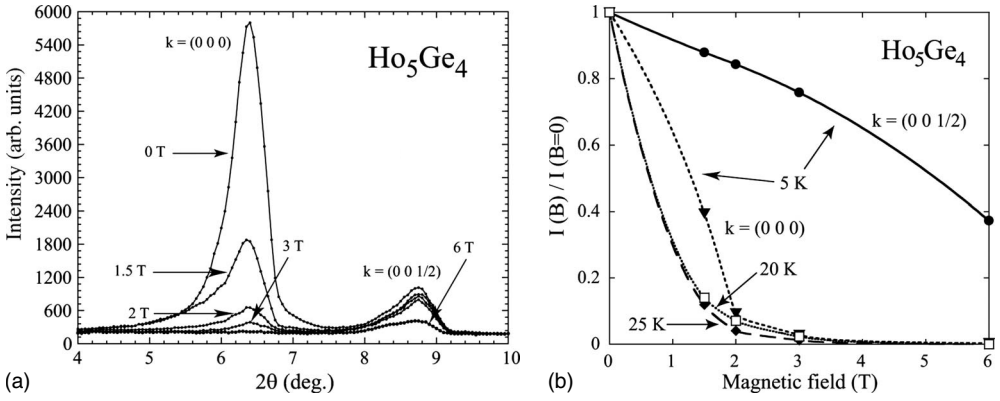

FIG. 13. (a) Magnetic-field dependence of the main magnetic peaks associated with the propagation vectors $\mathbf{k}=(0\ 0\ 0)$ and $\mathbf{k}=(0\ 0\ \frac{1}{2})$ in the AFM state of Ho_5Ge_4. (b) Normalized integrated intensities of these two peaks as a function of the magnetic field and the temperature.

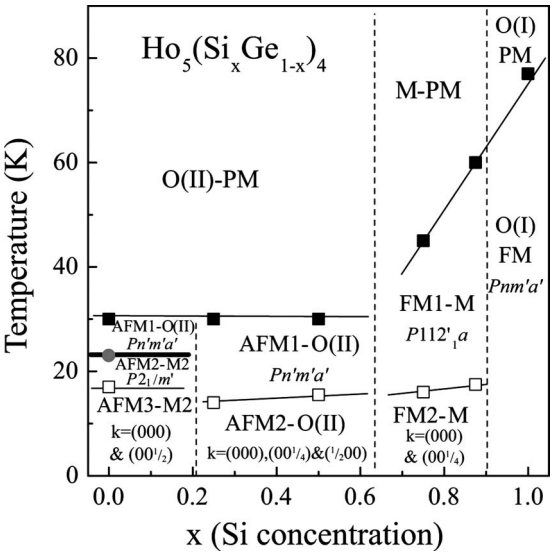

FIG. 14. Magnetic-crystallographic phase diagram of the system $Ho_5(Si_xGe_{1-x})_4$ summarizing the main results obtained in this work. The position of each of the studied compounds in the x axis is orientative. Double thick lines have been used in magnetic-structural transitions, single thick lines in the main magnetic ordering transitions, and thin lines in the secondary magnetic changes in ordered states. In addition to the conventional symbols for the crystal and magnetic states, the symbol M2 has been used to identify the $P2_1m$ monoclinic phase in Ho_5Ge_4. The sets of three numbers in parenthesis represent the magnetic propagation vectors existing in each magnetic state.

down to the lowest temperature ($T=2$ K). Ho_5Si_4 crystallizes in the O(I) Gd_5Si_4-type *Pnma* orthorhombic structure while the composition $x=0.75$ exhibits the *M* $Gd_5Si_2Ge_2$-type $P112_1/a$ monoclinic state and the composition $x=0.5$ crystallizes in the O(II) Sm_5Ge_4-type *Pnma* orthorhombic structure. Ho_5Si_4 undergoes a second order FM transition at $T_C=77$ K into a noncollinear FM structure with the magnetization oriented mainly along the a direction and weak AFM coupling along the b and c axis, $\mathbf{k}=(0\ 0\ 0)$. Ho_5Si_3Ge orders FM at $T_C=50$ K again with $\mathbf{k}=(0\ 0\ 0)$. At $T_C'\sim 16$ K a second magnetic transition sets in which evolves into a second commensurate magnetic phase with a propagation vector $\mathbf{k}=(0\ 0\ \frac{1}{4})$ below 8 K. The magnetic structure of the main $\mathbf{k}=(0\ 0\ 0)$ magnetic phase shows the dominance of a FM coupling along the a axis with an AFM canting along c. Similarly to other 5:4 monoclinic compounds, the magnetic moments located close to the covalent-like Si(Ge)-Si(Ge) bonds are larger than those placed near the broken bonds reflecting the bonding-related strengthening of the FM coupling. $Ho_5Si_2Ge_2$ exhibits a very complex low-temperature magnetic structure. In addition to the Nèel transition of the O(II) main phase at $T_N\sim 30$ K, two additional magnetic phases with the propagation vectors $\mathbf{k}=(0\ 0\ \frac{1}{4})$ and $\mathbf{k}=(\frac{1}{2}\ 0\ 0)$ are found at 15 and 12 K, respectively. The fit of the diffractogram at 2 K excluding most of the magnetic peaks stemming from these two incommensurate magnetic phases determines the magnetic space group of the main $\mathbf{k}=(0\ 0\ 0)$ magnetic phase to $Pn'm'a'$.

Ho_5Ge_4 orders antiferromagnetically at $T_N\sim 30$ K in the magnetic space group $Pn'm'a'$ with a propagation vector $\mathbf{k}=(0\ 0\ 0)$. Strong anisotropic strain develops on lowering the temperature reflecting the distribution of a and c lattice parameters preceding a new phase transition. This strain seems to be triggered by the upcoming magnetism and leads to a symmetry reduction. At 20 K, the crystal structure of Ho_5Ge_4 is described in the monoclinic space group $P2_1/m$ as already reported by Singh *et al.* The magnetic structure at this temperature can still be described with the magnetic propagation vector $\mathbf{k}=(0\ 0\ 0)$, but it is strongly anisotropic with two out of six Ho positions nonmagnetic. A second propagation vector $\mathbf{k}=(0\ 0\ \frac{1}{2})$ emerges at about 18 K whose coupling induces magnetism in the nonmagnetic Ho sites. Neutron diffractograms collected in applied magnetic field have demonstrated that ferromagnetism sets in Ho_5Ge_4 with the fast disappearance of the $\mathbf{k}=(0\ 0\ 0)$ propagation vector. On the other hand, the intensity associated with the state $\mathbf{k}=(0\ 0\ \frac{1}{2})$ decreases more slowly and about a 40% of the intensity is left at 6 T. As this phenomena occurs simultaneously with the field-induced segregation of a new low-temperature O(II) phase, their common evolution suggests a possible relationship between the amount of phase presenting the magnetic coupling $\mathbf{k}=(0\ 0\ \frac{1}{2})$ and the percentage of remnant $P2_1/m$ phase.

ACKNOWLEDGMENTS

The financial support of the Spanish MEC (Grant No. MAT2008-06567-CO2) and Spanish DGA (Grant No. E26) is acknowledged. C.M. acknowledges the Fundación Ramón Areces for funding part of this work with the postdoctoral grant "Beca para ampliación de estudios en universidades y centros de investigación en el extranjero en el campo de las Ciencias de la Naturaleza (2006–2007). Work supported in part by the Project No. POCI/CTM/61284/2004 and FEDER/POCTI Grant No. 155/94 from Fundação para a Ciência e Tecnologia (FCT). André Pereira is thankful for a PhD Grant (Grant No. SFRH/BD/22373/2005) from FCT, Portugal.

*Corresponding author. FAX: 34-976-762776; cmagend@unizar.es

[1] V. K. Pecharsky and K. A. Gschneidner, Jr., Phys. Rev. Lett. **78**, 4494 (1997).

[2] V. K. Pecharsky and K. A. Gschneidner, Jr., Appl. Phys. Lett. **70**, 3299 (1997).

[3] L. Morellon, Z. Arnold, C. Magen, C. Ritter, O. Prokhnenko, Y. Skorokhod, P. A. Algarabel, M. R. Ibarra, and J. Kamarad, Phys. Rev. Lett. **93**, 137201 (2004).

[4] L. Morellon, P. A. Algarabel, C. Magen, and M. R. Ibarra, J. Magn. Magn. Mater. **237**, 119 (2001).

[5] L. Morellon, C. Ritter, C. Magen, P. A. Algarabel, and M. R. Ibarra, Phys. Rev. B **68**, 024417 (2003).

[6] L. Morellon, P. A. Algarabel, M. R. Ibarra, J. Blasco, B. Garcia-Landa, Z. Arnold, and F. Albertini, Phys. Rev. B **58**, R14721 (1998).
[7] J. Stankiewicz, L. Morellon, P. A. Algarabel, and M. R. Ibarra, Phys. Rev. B **61**, 12651 (2000).
[8] E. M. Levin, V. K. Pecharsky, and K. A. Gschneidner, Jr., Phys. Rev. B **63**, 174110 (2001).
[9] J. B. Sousa, M. E. Braga, F. C. Correia, F. Carpinteiro, L. Morellon, P. A. Algarabel, and M. R. Ibarra, Phys. Rev. B **67**, 134416 (2003).
[10] E. M. Levin, K. A. Gschneidner, Jr., and V. K. Pecharsky, Phys. Rev. B **65**, 214427 (2002).
[11] C. Magen, L. Morellon, P. A. Algarabel, C. Marquina, and M. R. Ibarra, J. Phys.: Condens. Matter **15**, 2389 (2003).
[12] S. B. Roy, M. K. Chattopadhyay, P. Chaddah, J. D. Moore, G. K. Perkins, L. F. Cohen, K. A. Gschneidner, Jr., and V. K. Pecharsky, Phys. Rev. B **74**, 012403 (2006).
[13] C. Magen, P. A. Algarabel, L. Morellon, J. P. Araújo, C. Ritter, M. R. Ibarra, A. M. Pereira, and J. B. Sousa, Phys. Rev. Lett. **96**, 167201 (2006).
[14] L. Morellon, Z. Arnold, P. A. Algarabel, C. Magen, M. R. Ibarra, and Y. Skorokhod, J. Phys.: Condens. Matter **16**, 1623 (2004).
[15] C. Magen, L. Morellon, Z. Arnold, P. A. Algarabel, C. Ritter, M. R. Ibarra, J. Kamarad, A. O. Tsokol, K. A. Gschneidner, Jr. and V. K. Pecharsky, Phys. Rev. B **74**, 134427 (2006).
[16] A. O. Pecharsky, K. A. Gschneidner, Jr., V. K. Pecharsky, and C. E. Schindler, J. Alloys Compd. **338**, 126 (2002).
[17] Y. Mozharivskyj, A. O. Pecharsky, V. K. Pecharsky, and G. J. Miller, J. Am. Chem. Soc. **127**, 317 (2005).
[18] F. Holtzberg, R. J. Gambino, and T. R. McGuire, J. Phys. Chem. Solids **28**, 2283 (1967).
[19] N. P. Thuy, Y. Y. Chen, Y. D. Yao, C. R. Wang, S. H. Lin, J. C. Ho, T. P. Nguyen, P. D. Thang, J. C. P. Klaasse, N. T. Hien, and L. T. Tai, J. Magn. Magn. Mater. **262**, 432 (2003).
[20] A. M. Pereira, J. B. Sousa, J. P. Araujo, C. Magen, P. A. Algarabel, L. Morellon, C. Marquina, and M. R. Ibarra, Phys. Rev. B **77**, 134404 (2008).
[21] N. K. Singh, D. Paudyal, Ya. Mudryk, V. K. Pecharsky, and K. A. Gschneidner, Jr., Phys. Rev. B **79**, 094115 (2009).
[22] P. Schobinger-Papamantellos and A. Niggli, J. Phys. Colloq. **40**, C5-156 (1979).
[23] J. Rodriguez-Carvajal, Physica B **192**, 55 (1993); J. L. Rodriguez-Carvajal and T. Roisnel, http://www.ill.eu/sites/fullprof/
[24] V. H. Nguyen, A. Barlet, and J. Laforest, J. Phys. Colloq. **32**, C1-1133 (1971).
[25] A. S. Wills, Physica B **276-278**, 680 (2000).
[26] P. Schobinger-Papamantellos, J. Phys. Chem. Solids **39**, 197 (1978).
[27] C. Ritter, C. Magen, L. Morellon, P. A. Algarabel, M. R. Ibarra, V. K. Pecharsky, A. O. Tsokol, and K. A Gschneider, Jr., J. Phys.: Condens. Matter **18**, 3937 (2006).